

# Neutrinos from stochastic acceleration in black hole environments

Martin Lemoine<sup>1</sup> and Frank Rieger<sup>2,3</sup>

<sup>1</sup> Astroparticule et Cosmologie (APC), CNRS - Université Paris Cité, 75013 Paris, France  
e-mail: mlemoine@apc.in2p3.fr

<sup>2</sup> Max Planck Institute for Plasma Physics (IPP), Boltzmannstraße 2, 85748 Garching, Germany

<sup>3</sup> Institute for Theoretical Physics, Heidelberg University, Philosophenweg 12, 69120 Heidelberg, Germany  
e-mail: frank.rieger@ipp.mpg.de

December 3, 2024

## ABSTRACT

Recent experimental results from the IceCube detector and their phenomenological interpretation suggest that the magnetized turbulent corona of nearby X-ray luminous Seyfert galaxies can produce  $\sim 1 - 10$  TeV neutrinos via photo-hadronic interactions. In the present paper, we investigate in detail the physics of stochastic acceleration in such environments and examine under which conditions one can explain the inferred proton spectrum. To do so, we borrow recent findings on particle acceleration in turbulence and pay particular attention to the transport equation, notably for what concerns transport in momentum space, turbulent transport outside of the corona and advection through the corona. We first remark that the spectra obtained are highly sensitive to the value of the acceleration rate, e.g., to the Alfvénic velocity. Then we examine three prototype scenarios, one describing turbulent acceleration in the test-particle picture, one in which particles are pre-accelerated by turbulence and further energized by shear acceleration, and one in which we consider the effect of particle backreaction on the turbulence (damping), which self-regulates the acceleration process. We show that it is possible to obtain satisfactory fits to the inferred proton spectrum in all three cases, but stress that in the first two, the energy content in supra-thermal protons has to be fixed in an ad-hoc manner to match the inferred spectrum, at an energy density close to that contained in the turbulence. Interestingly, self-regulated acceleration by turbulence damping naturally brings the suprathermal particle energy content close to that of the turbulence and allows to reproduce the inferred flux level without additional fine tuning. We also suggest that, given the strong sensitivity of the maximal proton energy to the Alfvénic velocity (or acceleration rate), any variation of that quantity in the corona could affect, and in fact set the slope of the high-energy proton spectrum.

**Key words.** Acceleration of particles – Turbulence – Black hole physics – Magnetohydrodynamics (MHD)

## 1. Introduction

Supermassive black holes in active galactic nuclei (AGN) have long been regarded as potential accelerators to extreme energies (e.g., Eichler 1979a; Berezhinsky & Ginzburg 1981; Protheroe & Szabo 1992), whether in the accretion disk itself (e.g., Dermer et al. 1996; Aharonian & Neronov 2005; Lynn et al. 2014; Kimura et al. 2019b,a), in the magnetosphere (e.g., Levinson & Boldt 2002; Aharonian et al. 2002), around the base of the jet (e.g., Rieger & Mannheim 2000, 2002; Rieger & Aharonian 2009), or more recently through tidal disruption events (e.g., Farrar & Piran 2014; Guépin et al. 2018; Murase et al. 2020b; Winter & Lunardini 2023).

The recent announcement of a correlation of the arrival directions of (a subset of) high-energy ( $\epsilon_\nu \gtrsim 1 - 10$  TeV) neutrinos with local AGNs, in particular from the nearby ( $d \sim 10$  Mpc) Seyfert galaxy NGC 1068 (IceCube Collaboration et al. 2022; Halzen 2023; Abbasi et al. 2024a), has put these theoretical considerations on solid footing, triggered a surge of interest in these systems and more generally paved the way for a novel view on the origin of high-energy neutrinos (Neronov et al. 2024; Padovani et al. 2024). If confirmed, the detection of these neutrinos, with a flux an order of magnitude higher than the gamma-ray flux that would be expected in association, suggests that they have been produced through hadronic interactions of protons with energies  $\epsilon_p \gtrsim 30$  TeV in compact environments, where gamma-gamma absorption through pair pro-

duction becomes large enough to limit the outgoing gamma-ray flux (Murase et al. 2020a). Particle acceleration can be envisaged at accretion shocks, in the magnetized turbulence, through magnetic reconnection or through a combination of these processes (Murase et al. 2020a; Inoue et al. 2020; Kheirandish et al. 2021; Murase 2022; Eichmann et al. 2022; Fang et al. 2023; Fiorillo et al. 2024b; Murase et al. 2024; Mbarek et al. 2024; Fiorillo et al. 2024a; Das et al. 2024; Ambrosone 2024). In principle, given that the corona is strongly magnetized and turbulent, stochastic acceleration emerges as prime candidate. The main uncertainty that shrouds the expected ion and secondary neutrino spectra in that context stems from the modelling of particle acceleration and from the description of the corona itself.

Several authors have recently pointed out tensions between the magnitude of the neutrino flux inferred from NGC 1068 and that expected from the overall population (i.e., NGC 1068 should be significantly more luminous than other Seyferts, see Waxman 2024), and with the available energy budget of the NGC 1068 corona itself (Inoue et al. 2024). Pending confirmation of the IceCube results, which so far reach the  $4.2\sigma$  confidence level, we take these observations at face value and provide in the present paper a fresh and detailed discussion of stochastic acceleration in a turbulent magnetized corona, in order to discuss under which conditions one can recover the overall flux and spectral shape observed. To do so, we borrow recent insights into the physics of particle acceleration in turbulent and sheared velocity flows, to investigate the rate of acceleration in the turbulent corona and

at the base of the black hole outflow. Regarding stochastic acceleration, we pay particular attention to the transport equation and we address the possible backreaction of accelerated particles on the turbulence and its consequences for phenomenology. As we discuss further on, this backreaction, which generically leads to the damping of the turbulence and therefore to the modification of the accelerated particle spectra (e.g., Lemoine et al. 2024, and references therein), appears likely given the large ion energy flux inferred from IceCube data. We also examine the possible re-acceleration of particles by shear acceleration at the base of the jet, close to the black hole. We indeed have in mind a hierarchical picture in which particles can be accelerated by differing processes depending on their energy. This picture is motivated by the vast gap that separates the kinetic scales (e.g., the gyroradius of thermal ions  $r_L = 3 \times 10^3$  cm for a 1 GeV proton in a magnetic field of strength  $B = 10^3$  G) from the macroscopic scale of the source (e.g., the black hole gravitational radius  $r_g \equiv GM/c^2 \simeq 1.5 \times 10^{12} M_7$  cm)<sup>1</sup>. In such environments, pre-acceleration in reconnecting current sheets is generic and it can energize ions up to a Lorentz factor of the order of  $\sigma$ , the magnetization parameter defined as the ratio between magnetic and plasma energy density (Werner et al. 2018). Unless  $\sigma$  takes very large values (e.g., Fiorillo et al. 2024b; Mbarek et al. 2024), particles must draw most of their energy from their interaction with the turbulence. However, as they gain energy, their mean free path increases, so much that they may eventually become sensitive to the coherent, shear structure of the velocity flow around the black hole and hence be further energized through shear acceleration (e.g., Rieger 2019).

We thus adopt this point of view in the present paper and focus on the following key questions: under which conditions can such sources push protons to  $\sim 30 - 300$  TeV energies, and to which extent can they account for the spectrum inferred from IceCube neutrino observations. Correspondingly, we do not seek to reproduce the multi-wavelength spectrum observed from the prototype NGC 1068, which has been discussed and modeled to fine levels of detail in the aforementioned references (Murase et al. 2020a; Inoue et al. 2020; Kheirandish et al. 2021; Murase 2022; Eichmann et al. 2022; Fang et al. 2023; Fiorillo et al. 2024b; Murase et al. 2024; Mbarek et al. 2024; Fiorillo et al. 2024a; Das et al. 2024). However, we properly implement the associated rates of energy loss that limit the acceleration of multi-TeV to PeV protons.

This paper is organized as follows. In Sec. 2, we discuss the implementation of particle acceleration, first in a turbulent hot corona, then in a sheared velocity flow and show that various parameters control the ion energy spectra. We discuss the results in Sec. 3 and provide three types of scenarios to reproduce the inferred high-energy proton spectra: one considering stochastic acceleration in turbulence, one combining stochastic acceleration with shear acceleration, and a third involving stochastic acceleration, properly accounting for the feedback of accelerated particles on the turbulence. We emphasize that in the first two scenarios, different sources should exhibit (possibly largely) different spectra, given the strong dependence of the derived spectra on the physical conditions (e.g., the Alfvénic velocity  $v_A$ ). We also argue that self-regulation of the stochastic acceleration by turbulence damping provides a well motivated, satisfactory fit to the inferred spectrum without requiring ad hoc normalization of the flux of high-energy ions. This opens new avenues of research

into the physics of these cosmic accelerators. We summarize our findings in Sec. 4.

## 2. Modeling particle acceleration

### 2.1. Radiation fields and general set-up

We consider a generic setup in which a supermassive black hole of mass  $M_{\text{BH}}$  and size  $r_g$  is embedded in a luminous accretion-disc ( $L_{\text{disk}}$ ) corona environment. For simplicity, the corona that encompasses the main disk is assumed to be quasi-spherical and compact, of characteristic length  $r_{\text{co}} \leq 100r_g$  (e.g., Fabian et al. 2015). In contrast to the disc, the corona is taken to be hot, with proton temperatures up to virial, i.e.,  $T_p \simeq 1.2 \times 10^{11} (30/\hat{r})$  K, where  $\hat{r} \equiv r/r_g$ . While still high, radiative cooling results in electron temperatures that are significantly smaller ( $T_e \ll T_p$ ) as evidenced by the observed X-ray spectral cutoffs ( $\epsilon_{\text{cX}}$  at tens to hundreds of keV (e.g., Kamraj et al. 2018, 2022; Kammoun et al. 2024). In principle, energy dissipation through reconnection in magnetically dominated regions could represent an important means to maintain such electron temperatures (e.g., Di Matteo et al. 1997; Merloni & Fabian 2001; Liu et al. 2002; Sironi & Beloborodov 2020). Characteristic coronal plasma beta ( $\beta_p = p_{\text{gas}}/p_{\text{mag}}$ ) are expected to be of order unity, but likely decreasing with increasing distance away from the mid-plane (e.g., De Villiers et al. 2003, 2005). While AGN corona have commonly been thought to be optically thin ( $\tau_T < 1$ ) (Zdziarski 1985; Stern et al. 1995), recent modelling suggests that in some sources  $\tau_T$  may reach values up to some few (e.g., Kara et al. 2017; Kamraj et al. 2022). Characteristic Alfvén speeds are of the order  $v_A \simeq 0.15 (30/\hat{r})^{1/2} \beta_p^{-1/2} c$ , making efficient stochastic acceleration feasible<sup>2</sup>. In terms of  $\beta_p$ , the thermal plasma beta parameter, the corona magnetic field may reach strengths of  $B = \sqrt{8\pi n_p m_p c^2 / (3\hat{r}\beta_p)} \simeq 4 \times 10^3 (30/\hat{r}) M_7^{-1/2} \beta_p^{-1/2} \tau_T^{1/2}$  G where  $\tau_T = n_p \sigma_T r_c$  (cf., Padovani et al. 2024). In general, however, there are uncertainties as the physical origin of the corona and its emission is not well understood. In particular, magnetic field estimates based on the detection of coronal radio synchrotron emission (hybrid corona), for example, rather suggest  $B \sim \mathcal{O}(10)$  G on scales of  $\sim 80r_g$  (Inoue & Doi 2018; Inoue et al. 2020). It seems conceivable that the magnetic field decays away from the mid-plane. In the following we take  $B = 10^3$  G as reference value for the corona in application for NGC 1068. We will discuss implications for varying fields but already note that most of our results are insensitive to this choice. Unless the magnetic field takes values well in excess of  $10^4$  G, proton synchrotron losses can indeed be safely neglected. Furthermore, the rate of acceleration in stochastic acceleration is quantified by  $v_A$  and  $\ell_c$  (the outer scale of the turbulence), not by  $B$  per se. The strength of the magnetic field enters the expression for the particle mean free path, which controls escape losses and the efficiency of shear acceleration but with an exponent of  $\sim 1/3$  (see Appendix A).

As mentioned above, we focus on the suprathermal proton spectra produced by turbulent and/or shear acceleration and discuss to what extent this can reproduce a spectrum as inferred from the IceCube observations of NGC 1068 (IceCube Collaboration et al. 2022). This proton spectrum has a generic spectral index  $s \sim -3$  in the energy interval  $\sim 30 - 300$  TeV, and its normalization is such that the suprathermal particle pressure at  $\sim 30$  TeV should carry a fraction from  $\sim 0.01$  to  $\sim 0.3$  of the total

<sup>1</sup> All throughout, we use the usual shorthand notation  $Q_x = Q/10^x$ , where  $Q$  is expressed in cgs units, with the exception of solar masses for  $M$ .

<sup>2</sup>  $v_A$  sets the characteristic velocity of turbulent eddies on the outer scale, as we assume a strongly turbulent corona with  $\delta B \sim B$  and  $\beta_p \sim 1$ .

plasma pressure (Murase et al. 2020a; Kheirandish et al. 2021; Eichmann et al. 2022; Das et al. 2024). In the figures that follow, we will express the energy spectra in units of  $p_{\text{gas}}$  and accordingly normalize the butterfly diagram characterizing the inferred proton energy spectrum to 0.3, corresponding to a pressure ratio of 0.1. Given the experimental and modelling uncertainties, this normalization is itself uncertain to within a factor of a few.

## 2.2. Particle acceleration in turbulence

Stochastic particle acceleration has received increased attention in recent years, with notable inputs from numerical simulations (Zhdankin et al. 2017; Isliker et al. 2017; Pecora et al. 2018; Comisso & Sironi 2018, 2019; Kimura et al. 2019b; Zhdankin et al. 2019; Wong et al. 2020; Trotta et al. 2020; Bresci et al. 2022; Pezzi et al. 2022; Comisso & Sironi 2022; Pugliese et al. 2023), as well as theoretical developments (Lynn et al. 2014; Brunetti & Lazarian 2016; Lemoine 2019; Lemoine & Malkov 2020; Demidem et al. 2020; Sioulas et al. 2020b,a; Lemoine 2021, 2022; Xu & Lazarian 2023).

In phenomenological applications, stochastic acceleration is commonly modeled through a purely diffusive Fokker-Planck equation, characterized by a (energy-dependent) diffusion coefficient  $D_{\epsilon\epsilon}$ , an approach mostly motivated by simplicity and by arguments borrowed from a quasilinear description of weak turbulence theory (e.g., Schlickeiser 1989). In such an approach, all information regarding the acceleration rate is encoded in the diffusion coefficient  $D_{\epsilon\epsilon}$ , in particular the acceleration rate  $v_{\text{acc}} \equiv D_{\epsilon\epsilon}/\epsilon^2$ . The general transport equation that describes the evolution of the particle distribution  $n_\epsilon \equiv dn/d\epsilon$  then takes the form

$$\partial_t n_\epsilon = \mathcal{L}_{\text{stoch}} n_\epsilon - \partial_\epsilon (\dot{\epsilon}_{\text{loss}} n_\epsilon) - \frac{n_\epsilon}{\tau_{\text{esc}}}, \quad (1)$$

where  $\mathcal{L}_{\text{stoch}}$  denotes the diffusive operator describing stochastic acceleration, i.e.

$$\mathcal{L}_{\text{stoch}} n_\epsilon \equiv \partial_\epsilon (D_{\epsilon\epsilon} \partial_\epsilon n_\epsilon) - 2\partial_\epsilon (D_{\epsilon\epsilon} n_\epsilon / \epsilon) \quad (2)$$

for the purely diffusive Fokker-Planck scheme. In equation (1),  $\dot{\epsilon}_{\text{loss}}$  denotes the proton energy loss rate (here, a negative quantity by convention) associated with Bethe-Heitler pair production  $p\gamma \rightarrow e^-e^+$ , and hadronic  $p-p$  and  $p-\gamma$  interactions that lead to neutrino production. These energy losses become significant at energies  $\epsilon \gtrsim 10$  TeV, see, e.g., Murase (2022), and their implementation is discussed in Appendix A.

The timescale  $\tau_{\text{esc}}$  characterizes the time over which particles escape from the acceleration region through spatial diffusion. In a highly dynamic turbulence, it is important to keep in mind that particle transport can occur both through scattering on magnetic inhomogeneities (with mean free path  $\lambda_{\text{scatt}}$ ), and through turbulent transport, with characteristic diffusion coefficient  $\kappa_{\text{turb}} \sim \ell_c v_A/3$ . As the scattering mean free path is of order  $\lambda_{\text{scatt}} \sim r_L^{1/3} \ell_c^{2/3}$  (see Appendix A), in practice diffusive escape is governed by turbulent transport. This point seems to have gone mostly unnoticed, even though it brings important constraint on the geometry of the corona. A large  $\ell_c$  diminishes the acceleration rate but increases the escape rate, while a large  $v_A$  increases both acceleration and escape rates. For definiteness, we adopt a diffusion coefficient  $\kappa = \kappa_{\text{turb}} + \lambda_{\text{scatt}} c/3$  and discuss consequences in Sec. 3. The diffusive escape timescale is then written  $\tau_{\text{esc}} \equiv r_{\text{co}}^2 / (2\kappa)$ .

Additionally, we also take into account the influence of particle escape out of the accelerating region through advective transport. To do so, we bound the integration time to  $\tau_{\text{adv}}$ , which is

defined in terms of the advection velocity  $v_{\text{adv}}$  as  $\tau_{\text{adv}} \equiv r_{\text{co}}/v_{\text{adv}}$ . Thus, we do not seek, from the outset, a stationary solution to the transport equation Eq. (1). In our formulation, the proton spectrum achieves stationarity because the injection is itself stationary in time. Specifically, at any given time  $t$ , the proton spectrum contained in the turbulent corona is made of particles that have been injected at times  $t' \in [t - \tau_{\text{adv}}, t]$  and accelerated for a duration  $\tau \equiv t - t'$ . This spectrum can be expressed as

$$\frac{dn_{\text{cor}}}{d\epsilon} = \int_0^{\tau_{\text{adv}}} d\tau \int_0^{+\infty} d\epsilon' G_{\text{turb}}(\epsilon; \epsilon', \tau) \frac{d\dot{n}_{\text{inj}}}{d\epsilon'}, \quad (3)$$

in terms of the Green's function  $G_{\text{turb}}(\epsilon; \epsilon', \tau)$  associated to Eq. (1), which determines the probability of transiting from  $\epsilon'$  to  $\epsilon$  over a time interval  $\tau$ , and of the injection rate spectrum  $d\dot{n}_{\text{inj}}/d\epsilon$ . We assume that the latter is constant in time, and as discussed further on, monoenergetic without loss of generality.

The above implementation accommodates equally well injection of particles at one side of the corona, then advection, or uniform stationary injection throughout the corona. In both cases,  $dn_{\text{cor}}/d\epsilon$  can be regarded as the stationary average spectrum. In the former case, the time-dependent spectrum at location  $x$  can be written  $dn_{\text{turb}}(x)/d\epsilon = \int d\epsilon' G_{\text{turb}}(\epsilon; \epsilon', x/v_{\text{adv}}) dn_{\text{inj}}/d\epsilon'$  in terms of the injection density  $dn_{\text{inj}}/d\epsilon'$  at the initial boundary, and the substitutions  $x \rightarrow v_{\text{adv}}\tau$ ,  $dn_{\text{inj}}/d\epsilon' \rightarrow \tau_{\text{adv}} d\dot{n}_{\text{inj}}/d\epsilon'$  leads to Eq. (3) above, where the time integral represents an average over the corona. In the latter case, particles are injected throughout the corona at rate  $d\dot{n}_{\text{inj}}/d\epsilon'$  (independent of  $x$ ), so that

$$\frac{dn_{\text{turb}}(x)}{d\epsilon} = \int_0^x \frac{dx'}{v_{\text{adv}}} \int_0^{+\infty} d\epsilon' G_{\text{turb}}(\epsilon; \epsilon', (x-x')/v_{\text{adv}}) \frac{d\dot{n}_{\text{inj}}}{d\epsilon'}. \quad (4)$$

Then,  $dn_{\text{cor}}/d\epsilon$  is again recovered by taking the average of  $dn_{\text{turb}}(x)/d\epsilon$  over  $x$  throughout the corona.

The advection term is sometimes included in the transport equation as an escape term of the form  $-n_\epsilon/\tau_{\text{adv}}$ , which implicitly implies that particles can spend a time  $> \tau_{\text{adv}}$  in the acceleration region and thus get accelerated to much higher energies. However, advection is a systematic loss, not a random one, and it must therefore be treated differently. This impacts the particle spectra in a significant way. In the present description, in particular, advection effectively cuts off the spectrum at a maximal energy set by  $v_{\text{acc}}\tau_{\text{adv}} \sim 1$  (or below, if other losses dominate).

Recent numerical experiments of stochastic particle acceleration, which either track test particles in an MHD simulation, or rely on a full kinetic description using the particle-in-cell (PIC) technique, have revealed a richer and complex landscape than the simple above Fokker-Planck formulation. These simulations point to a diffusion coefficient of the form  $D_{\epsilon\epsilon} \simeq 0.2\gamma^2(v_A/c)^2 c/\ell_c$  for particles of Lorentz factor  $\gamma \equiv \epsilon/mc^2$ , where  $v_A$  denotes the Alfvén velocity in the total magnetic field and  $\ell_c$  the coherence length of the turbulence. However, they also demonstrate that the purely diffusive Fokker-Planck approach does not successfully account for the particle spectra (Isliker et al. 2017; Pecora et al. 2018; Lemoine & Malkov 2020), unless one adds an energy-dependent (as well as  $v_A$ -dependent) advection coefficient, which must be extracted from numerical simulations (Wong et al. 2020). This is not a trivial issue, because one must extrapolate far in time the results of these kinetic simulations in order to make connection with phenomenology. For instance, for our fiducial values  $v_{\text{adv}} = 0.02c$ ,  $r_{\text{co}} = 30r_g$  and  $\ell_c = 10r_g$ , the advection/integration timescale reads  $\tau_{\text{adv}} \simeq 150\ell_c/c$ , while PIC simulations typically run over  $\simeq 10\ell_c/c$ .

In Lemoine (2021, 2022), we have argued that particles are accelerated through a generalized Fermi process, in which particles gain energy as they cross intermittent regions of dynamic, curved and/or compressed magnetic field lines. This model has been benchmarked on MHD simulations in a regime relevant to black hole coronae, namely a sub- to mildly relativistic Alfvénic velocity, and the time-dependent Green’s functions for the spectra obtained in this approach also match those seen in PIC simulations in similar conditions (Comisso & Sironi 2022). To account for the intermittent nature of the accelerating structures, it proves necessary to go beyond a purely diffusive Fokker-Planck treatment and to consider the full probability distribution function of the random forces acting on the particles. The transport can then be modelled using Eq. (1) above, with a more general diffusion operator characterized by

$$\mathcal{L}_{\text{stoch}} n_\epsilon \equiv \int_0^{+\infty} dt' \left[ \frac{\varphi(\epsilon|\epsilon')}{t'} n_{\epsilon'}(t) - \frac{\varphi(\epsilon'|\epsilon)}{t_\epsilon} n_\epsilon(t) \right], \quad (5)$$

where  $\varphi(\epsilon|\epsilon')$  represents the kernel describing the probability of jumping from  $\epsilon'$  to  $\epsilon$  over a time interval  $t'$ , as described in Lemoine (2022), see also Isliker et al. (2017) for related considerations. This kernel has been determined through dedicated measurements carried out in an MHD simulation with Alfvénic velocity  $v_A = 0.4 c$ . It can nevertheless be extrapolated to other Alfvénic velocities by rescaling its width in proportion to  $(v_A/0.4 c)^2$  and we do so in the following.

In order to leverage on these recent findings, and to gauge the influence of the underlying theoretical uncertainty on the predicted particle spectra, we adopt both pictures in the following, namely we integrate the transport equation (1) using either the Fokker-Planck kernel [Eq. (2), hereafter referred to as model (1)] or that describing the generalized Fermi process [Eq. (5), hereafter model (2)]. Our main motivation here is to provide a more accurate description of the proton and secondary neutrino spectra and of the corresponding acceleration rate.

For what concerns practical applications, the generalized Fermi process produces time-dependent Green’s functions that take the form of broken powerlaws in the absence of escape and losses. Such solutions obviously differ from the lognormal shape (e.g., Kardashev 1962) that follows from a purely diffusive Fokker-Planck kernel with  $D_{\epsilon\epsilon} \propto \epsilon^2$  (in the absence of escape and losses). Once continuous injection of particles is included, both formulations nevertheless lead to hard spectra beyond the injection Lorentz factor  $\gamma_0$  (Schlickeiser 1984), up to a maximal energy that is either dictated by the finite time ( $\tau_{\text{adv}}$ ) over which particle acceleration takes place, or by energy losses.

We do not discuss here the physics of injection and simply assume that a given number of particles is injected into turbulent acceleration with characteristic Lorentz factor  $\gamma_0 \sim 1$ . The value of this Lorentz factor, or the exact shape of the injected spectrum does not matter, since turbulent acceleration effectively loses dependence on the initial conditions once acceleration to high energies has taken place. This injection could either take place through magnetic reconnection in localized patches of sufficient magnetization (e.g., Mbarek et al. 2024), through fast, small-scale turbulent acceleration in localized regions, as observed in some simulations (e.g., Pecora et al. 2018; Trotta et al. 2020), or simply because a fraction of the energy density is contained in supra-thermal particles accelerated elsewhere and accreted into the corona. The exact energy fraction contained in these particles does matter, however, as we discuss in the following.

The spectral shape is controlled by the following parameters:  $D_{\epsilon\epsilon}$  or  $\varphi(\epsilon|\epsilon')$  for what concerns the acceleration rate, which

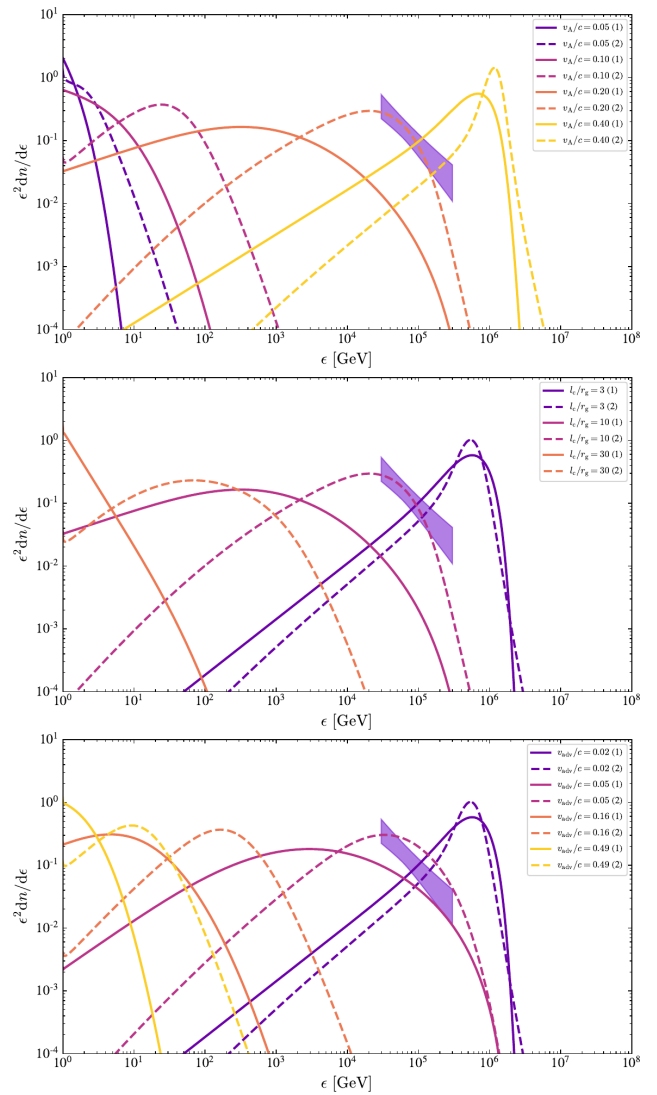


**Fig. 1.** Proton energy spectra  $\epsilon^2 dn_{\text{cor}}/d\epsilon$  (per log-interval of energy) vs proton energy  $\epsilon$  predicted by stochastic acceleration in a turbulent corona, starting from mono-energetic protons with Lorentz factor  $\gamma_0 \sim 1$ . In each panel, the solid line corresponds to a solution obtained by integrating the Fokker-Planck equation up to time  $\tau_{\text{adv}} = r_{\text{co}}/v_{\text{adv}}$  [model (1) including energy losses, advection and escape as described in the text], while the dashed line shows the corresponding solution for the same parameters for the generalized Fermi model described by Eq. (5) [model (2)]. In all panels,  $r_{\text{co}}$  is set to  $30 r_g$ ; in the top and middle panels,  $v_{\text{adv}} \approx 0.02 c$ . The upper panel shows the dependence on  $v_A$ , assuming otherwise a coherence length scale for the turbulence  $\ell_c = 10 r_g$  and an advection velocity  $v_{\text{adv}} = 0.02 c$ : from left to right, as indicated,  $v_A/c = 0.05$ ,  $v_A/c = 0.10$ ,  $v_A/c = 0.20$  and  $v_A/c = 0.40$ . The middle panel examines the dependence on  $\ell_c$ , assuming otherwise  $v_A/c = 0.20$  and  $v_{\text{adv}}/c = 0.02$ : from right to left, as indicated,  $\ell_c = 3 r_g$ ,  $\ell_c = 10 r_g$  and  $\ell_c = 30 r_g$ . The bottom panel examines the influence of advection, characterized here by the advection velocity  $v_{\text{adv}}$  (which sets the advection timescale  $\tau_{\text{adv}} \equiv r_{\text{co}}/v_{\text{adv}}$ ), assuming otherwise  $v_A/c = 0.20$  and  $\ell_c = 3 r_g$ : from right to left, as indicated,  $v_{\text{adv}}/c = 0.02$ ,  $v_{\text{adv}}/c = 0.05$ ,  $v_{\text{adv}}/c = 0.16$  and a (more extreme) case  $v_{\text{adv}}/c = 0.49$ . The butterfly indicates the range of values needed to reproduce a neutrino spectrum as observed by IceCube for NGC 1068. The energy density spectrum is expressed in units of the background plasma pressure, see Sec. 2.1. In these units, each individual spectrum has been normalized to an integrated fraction of unity, for the sake of illustration.

both depend on  $v_A$ ,  $\epsilon$  and  $\ell_c$ ;  $\tau_{\text{adv}} \equiv r_{\text{co}}/v_{\text{adv}}$  that sets the integration time before advective escape at velocity  $v_{\text{adv}}$  removes

the particles,  $\tau_{\text{esc}}$  and  $\tau_{\text{loss}}$  which control the timescales associated to diffusive escape and radiative energy losses. Regarding the latter, we follow previous treatments and recall their value in Appendix A. Figure 1 shows the results obtained for the Fokker-Planck model (solid lines) and the generalized Fermi process (dashed lines) for various choices of  $v_A$  (upper panel),  $\ell_c$  (middle panel) and  $v_{\text{adv}}$  (lower panel). The butterfly diagram shows the range of values inferred from the IceCube detection of neutrinos from NGC 1068, as discussed earlier on. Note that the energy spectra shown here is expressed in units of the background plasma pressure (Sec. 2.1). However (see also below), the spectra shown here have been normalized in an ad-hoc way to a total energy density of unity in those units. In general, turbulent acceleration allows for a favourable situation by yielding sufficiently hard spectra, which effectively minimizes the required energy budget if the peak occurs close to the observed energy range.

One should not be misled at this stage by the trivial observation that hardly any of the spectra fit this butterfly diagram. The important point is that the predicted spectra are extremely sensitive to the choice of parameters. This is easily understood, noting that for  $D_{\epsilon\epsilon} \propto \epsilon^2$ , the mean energy increases exponentially fast in time, i.e.,  $\langle \epsilon \rangle \propto \exp(4v_{\text{acc}}t)$ , with  $v_{\text{acc}} \equiv D_{\epsilon\epsilon}/\epsilon^2$  the acceleration rate defined earlier. Consequently, in a fixed time interval  $t = \tau_{\text{adv}}$  over which  $v_{\text{acc}}t \gg 1$  (needed to achieve acceleration to high energies), changing  $v_{\text{acc}}$  by a factor of a few changes the maximum energy by orders of magnitude. The dependence of  $v_{\text{acc}}$  on the parameters is recalled above,  $v_{\text{acc}} \propto v_A^2/\ell_c$ . Here, we have assumed  $\delta B/B \gtrsim 1$ , otherwise  $v_{\text{acc}}$  should be further suppressed by a factor  $(\delta B/B)^2$ . The dependence on advection velocity is also easily understood, given that the number of  $e$ -folds of increase of the maximum energy scales as  $v_{\text{acc}}\tau_{\text{adv}} \propto 1/v_{\text{adv}}$ . From this, one can also infer the dependence on the scale of the corona. The spectra that reach PeV energies cut off because of catastrophic hadronic losses. Other spectra cut off because of the limited time spent in the corona.

Obviously, one could find parameter values that fit the inferred butterfly diagram and examples will be shown later on. This, however, comes at the price of some fine-tuning. One important corollary is that, under the above assumptions, one should not expect all AGN, even those with similar X-ray luminosity, to produce neutrinos with a similar spectrum. Rather, if the physical conditions that dictate the rate of acceleration (e.g.,  $v_A$ ) shows an extended distribution over the neutrino-emitting AGN sub-population, the population as a whole should produce an extended neutrino energy spectrum, from  $\lesssim$  GeV to  $\sim 0.1$  PeV. This has both consequences for our prediction of the diffuse flux from such a population of AGN and for the modelling of the spectrum of a given source, as we discuss further in Sec. 3.

Another important lesson drawn from Fig. 1 is that fitting the inferred proton spectrum raises an energy budget issue, noted earlier (Sec. 2.1), which also represents an intriguing coincidence. Namely, in order to match the flux, one must inject into stochastic acceleration a tiny fraction of the thermal plasma, such that after energization by a factor  $\sim 10^5$ , it ends up with a pressure comparable to that of its parent population. Had more particles had been injected, the energy requirement would have become excessive, while in the opposite case, the proton flux fall short of that required. Moreover, if suprathermal particles carry an energy density comparable to that in the thermal component, they must backreact on the flow, and in particular damp the turbulence that feeds them in energy. In such a situation, stochastic acceleration becomes nonlinear and self-regulated by damping (Eilek 1979; Eichler 1979b; Litvinenko 2012; Kakuwa 2016;

Lemoine et al. 2024). We will discuss this possibility further in Sec. 3.

Alternatively, it may be that the turbulent corona does not shape all of the proton spectrum, only part of it, and that protons escaping the corona are further accelerated in the sheared velocity flows at the base of the jet. We first discuss how this shear acceleration can be implemented, then examine the general combination of the two scenarios in Sec. 3.

### 2.3. Particle acceleration in sheared flows

Accreting black hole systems are known to drive relativistic jets and winds, providing an environment conducive to shear-type particle acceleration (e.g., Rieger 2019; Lemoine 2019; Rieger & Duffy 2022; Webb et al. 2023; Wang et al. 2024). This could potentially provide a complementary mechanism for proton energization in case turbulent acceleration in the corona would saturate at multi-TeV energies. To be efficient, shear acceleration commonly requires seed injection of energetic particles, in line with a hierarchical acceleration scenario. In the present context, we envisage that the black hole vicinity supports a fast, sheared outflow, e.g., that the hot X-ray emitting corona forms the base of an outward-moving jet, whether radiation pressure supported or magnetically driven (e.g., Beloborodov 1999; Malzac et al. 2001; Merloni & Fabian 2002; King et al. 2017; Liska et al. 2022; Poutanen et al. 2023; Dexter & Begelman 2024). For the prototype Seyfert galaxy NGC 1068 jet-like features are indeed apparent on larger scales, though jet speeds are most likely non-relativistic ( $\lesssim 0.1c$ ) on scales of several tens of parsec ( $\sim 10^7 r_g$ ) from the nucleus (Gallimore et al. 1996; Roy et al. 2000). Part of its observed gamma-ray emission may in fact be jet-related (e.g., Lenain et al. 2010; Salvatore et al. 2024). The radio-inferred (large-scale and time-averaged) jet power is of the order of  $L_{\text{jet}} \sim 10^{43}$  erg/s (Padovani et al. 2024). On the other hand, the minimum (isotropic-equivalent) cosmic ray power required to account for the observed neutrino emission is of the order of several  $10^{42}$  erg/s (e.g., Muras 2022, see also Appendix A). If part of this emission is indeed outflow-related, even if relativistically boosted, it seems conceivable that cosmic-ray acceleration may contribute to the flow being decelerated (viscous drag) as it propagates outwards. We do not include in our modelling here this possible backreaction and self-regulation of the acceleration process, but note that it may impact on both, bulk flow profile (e.g., shear broadening) and turbulence generation.

For reference, we explore in the following a model where turbulent acceleration in the corona saturates at  $\gamma_p \leq 10^4$  (10 TeV), either due to  $v_A \lesssim 0.1c$  or  $\ell_c \gg r_g$  in the corona, the corona thus sustaining a reservoir of energetic seed particles that can diffuse into the outflow and experience further jet-shear acceleration. In this process acceleration is related to a particle effectively sampling the velocity difference while being scattered across a shearing flow (Rieger 2019). For simplicity, we consider a collimated, mildly relativistic outflow or jet, with Lorentz factor  $\gamma_j \equiv 1/(1 - u_z^2/c^2)^{1/2} \lesssim 3$ , characterised by a lateral velocity shear  $u_z(r)$  of width  $\Delta r = \hat{r}_{\text{sh}} r_g$ . Energetic protons undergoing shear acceleration will be subjected to radiative losses and diffusive escape (see Appendix A). For phenomenological application, the acceleration process can be modelled through a diffusive Fokker-Planck equation for  $n(\epsilon)$  of the type Eq. (1), with mean momentum diffusion coefficient  $D_{\epsilon\epsilon} \propto p^2 \bar{D}_p$ , where for energetic protons  $\epsilon = pc = \gamma m_p c^2$ . The coefficient  $\bar{D}_p \equiv a_g \lambda / c$  can be obtained from the local ( $r$ -dependent) shear coefficient  $D_p(r) = (1/15)\gamma_j(r)^4 (\partial u_z / \partial r)^2 \lambda / c$  by suitable spatial averaging,

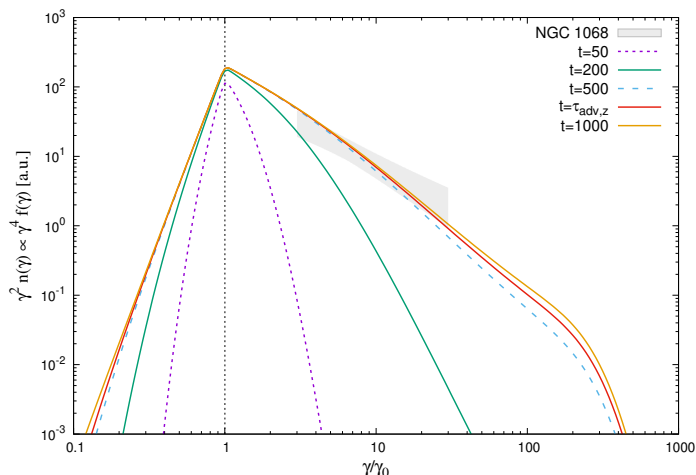


**Fig. 2.** Exemplary time-dependent proton energy distribution obtained from jet-shear acceleration with a Fokker-Planck model assuming continuous injection of seed protons with  $\gamma_0 = 10^4$ . As a result of advective escape, the predicted particle spectrum will appear somewhat softer (red,  $t = \tau_{\text{adv},z}$ ) compared to the otherwise quasi steady-state distribution (yellow). The grey-shaded region illustrates spectral characteristics required to reproduce the neutrino emission for NGC 1068 as measured by IceCube.

e.g.,  $a_g = (2/3)(c/\Delta r)^2/w$  with  $w = 116 (\ln[(1 + \beta_0)/(1 - \beta_0)])^{-2}$  in the case of a linearly decreasing shear flow profile with maximum (spine) speed  $\beta_0 = (1 - 1/\gamma_{j,\text{max}}^2)^{1/2}$  (Rieger & Duffy 2019, 2022). In the former expression,  $\lambda = c\tau_c = \eta(\Delta r)(r_L/\Delta r)^{1/3}$  denotes the scattering mean free path ( $r_L$  the gyroradius), for which we take a scaling with  $\eta = 2$ , following Rieger & Duffy (2019) and Wang et al. (2023), see also Appendix A. Particles can escape out of the acceleration region either due to cross-field diffusion (laterally), i.e.,  $\tau_{\text{esc}} = (\Delta r)^2/(2\kappa)$  with  $\kappa = \lambda c/3$ , or advective transport (along  $z$ ),  $\tau_{\text{adv},z}$ . What is of interest in the current context, is the accelerated particle distribution on scales of the corona. While shear acceleration likely continues to operate along the jet, we consider the former to dominate hadronic interactions and thus neutrino production. Accordingly, we approximate advective escape by  $\tau_{\text{adv},z} \approx z/\langle u_z \rangle = \tilde{z}r_{\text{co}}/\langle u_z \rangle$ , with  $\langle u_z \rangle$  the mean velocity (here corresponding to  $\beta_0 c/2$ ),  $\tilde{z} \equiv z/r_{\text{co}}$  less than a few to ensure a high enough target photon density. As before (Sec. 2.2), this is implemented as a constraint on the time available for particle acceleration. Figure 2 presents exemplary proton energy spectra as a function of time (in units of  $\tau_c(\gamma_0)$ ) assuming that seed protons are continuously injected with Lorentz factor  $\gamma_0 = 10^4$  into a shearing flow with  $\gamma_j = 3$ ,  $B = 50$  G,  $\hat{r}_{\text{sh}} = 2$  and  $\tilde{z} = 2$ , assuming a corona size of  $r_{\text{co}} = 30r_g$ .

In general, the predicted spectra are sensitive to the choice of parameters, e.g., the time available for particle acceleration (set by  $\tau_{\text{adv},z}$ ). One important corollary of the latter is that shear modelling imposes constraints on the size and geometry of the corona. In addition, the required maximum outflow speed to model the CR parent distribution behind the IceCube neutrino spectrum is sensitive to the flow profile. In comparison to power-law or Gaussian type velocity profiles, a linearly decreasing shear flow profile requires higher speeds to reproduce hard particle spectra. In fact, for the former  $\gamma_j \leq 2$  are sufficient (Rieger & Duffy 2022). This suggests that mildly relativistic outflow speeds are sufficient to account for the inferred proton spectrum in the case of NGC 1068. Our current model at this stage remains exploratory in nature since the innermost outflow characteristics

in Seyfert-2 AGNs remain uncertain, and since we neglected a possible shear contribution due to flow rotation. The latter may facilitate transport of angular momentum from the underlying accretion flow, and in effect contribute to further spectral hardening in sheared flows will not lead to a canonical power-law shape, faster flows will (ceteris paribus) result in harder particle spectra. This ties in with the above corollary according to which one should not expect all X-ray bright Seyfert AGN to have similar neutrino spectra.

### 3. Discussion

#### 3.1. Particle spectra

In the preceding section, we have examined the general features of particle acceleration in a turbulent corona, with possible re-acceleration in the sheared velocity flow outside of that corona. Here, we interpret these results, combine them to suggest ways of reproducing the generic proton spectrum inferred from IceCube observations, and draw conclusions regarding phenomenology. More specifically, we investigate the following three scenarios.

First, we consider pure stochastic acceleration in the turbulent corona, as modelled in Sec. 2.2, and demonstrate that a reasonable set of parameters can be found to reproduce the high-energy general slope. This was known from previous studies (e.g., Murase et al. 2020a; Inoue et al. 2020; Kheirandish et al. 2021; Murase 2022; Eichmann et al. 2022; Fiorillo et al. 2024a), the main novelty here lying in the transport equation used, in particular for what concerns the implementation of generalized Fermi acceleration, as well as the treatment of escape and advection. As noted above (Sec. 2.2), matching the spectrum requires some tuning, both in terms of the physical parameters and in terms of flux normalization, suggesting that other sources might display vastly different neutrino spectra even for otherwise similar coronal X-ray luminosities. Interestingly, the IceCube experiment reports differing spectra from other Seyfert galaxies (e.g., Abbasi et al. 2024a,b). In the case of NGC 4151 ( $d \sim 16$  Mpc), for instance, the characteristic neutrino energy seems a factor  $\sim 5$  larger and the high-energy slope slightly harder than in NGC 1068.

The spectra obtained in this first scenario are shown in the top panel of Fig. 3, with: in solid lines, the spectrum obtained from the Fokker-Planck model (1), and in dashed lines, the spectrum obtained from the generalized Fermi acceleration model (2). The parameters are the same for both:  $r_{\text{co}} = 30r_g$ ,  $\ell_c = 10r_g$ ,  $v_{\text{adv}} = 0.02c$  and  $v_A = 0.22c$  (resp.  $v_A = 0.20c$ ) for model 1 (resp. model 2). However, their flux normalizations are different. The ratio of integrated energy density of suprathermal particles to background plasma pressure is respectively  $\approx 4.3$  for model (1) and 1.0 for model (2). Given that the ratio of pressures is a factor 3 lower, the dynamical influence of the suprathermal particles should not be ignored in model (1). This further motivates the need to study the impact of backreaction on the turbulence, discussed further below. Finally, we note that other sets of parameters could be found, e.g., a lower Alfvén velocity with a smaller coherence length scale etc. However, the general spectral shape should be preserved.

In a second scenario, we investigate the interplay of turbulent and shear acceleration. Shear acceleration requires high-energy seed particles, because the rate at which acceleration proceeds increases with the particle mean free path (e.g. Rieger 2019; Rieger & Duffy 2022; Webb et al. 2023; Wang et al. 2024), so

that, in the absence of turbulent pre-acceleration, this mechanism would be effectively inefficient. In the present setting, particles that have been pre-accelerated in a turbulent corona are assumed to enter a region of sheared velocity flow, either through diffusive escape, or through advection from the corona. For the sake of definiteness, we concentrate here on the latter case, in which particles first cross a turbulent corona, then enter a region of sheared velocity flow. There is sizable uncertainty here, not only on the overall geometry of the problem, but also on the exact fraction of particles able to transit from one region to the next, as well as on the parameters characterizing the shear flow. We thus borrow the same parameters than those introduced in Sec. 2.3 describing the base of a mildly relativistic jet. To model the particle spectra, we convolve the Green's function that characterizes shear acceleration  $G_{\text{shear}}(\epsilon; \epsilon', \tau_{\text{shear}})$ , i.e. the probability of jumping from  $\epsilon'$  to  $\epsilon$  over the timescale  $\tau_{\text{shear}}$  spent in the shear region, with an injection distribution that describes the time-dependent particle spectrum coming out of the turbulent region. Denoting the latter as  $dn_{\text{turb}}/d\epsilon'$ , the stationary spectrum in the shear region is written

$$\frac{dn_{\text{shear}}}{d\epsilon} = \frac{1}{\tau_{\text{adv},z}} \int_0^{\tau_{\text{adv},z}} d\tau \int d\epsilon' G_{\text{shear}}(\epsilon; \epsilon', \tau) \frac{v_{\text{adv}}}{v_{\text{shear}}} \frac{dn_{\text{turb}}}{d\epsilon'}, \quad (6)$$

with  $\tau_{\text{adv},z}$  the advection time in the sheared region, as before, and

$$\frac{dn_{\text{turb}}}{d\epsilon'} = \int d\epsilon'' G_{\text{turb}}(\epsilon'; \epsilon'', \tau_{\text{adv}}) \frac{dn_{\text{inj}}}{d\epsilon''}, \quad (7)$$

where  $dn_{\text{inj}}/d\epsilon''$  characterizes as before (Sec. 2.2) the injection spectrum at the entry of the turbulent region. We have introduced a ratio  $v_{\text{adv}}/v_{\text{shear}}$  as a prefactor in Eq. (6) to account for the difference in advection velocity of each region (conservation of particle current). We assume that the shear region extends over  $r_{\text{co}}$  and take  $\langle u_z \rangle = \beta_0 c/2 \simeq 0.5 c$ .

Finally, the total stationary spectrum is obtained as the sum of the spectra in each region,  $dn_{\text{cor}}/d\epsilon$  [Eq. (3)] and  $dn_{\text{shear}}/d\epsilon$  [Eq. (6)]. Although the overall normalization is left here as a free parameter, the relative normalization of these two is fixed by the volume of each region. The result is shown in the middle panel of Fig. 3. The turbulent contribution is plotted in dotted line, that of the shear in dashed line, and the properly weighted sum of the two is shown as a thick solid line, further normalized to the butterfly diagram. The two sets of lines correspond to the models (1) and (2) used to describe stochastic acceleration in the turbulent part; model (1) assumes  $v_A/c = 0.20$ , while model (2) assumes  $v_A/c = 0.17$ .

This figure illustrates that the shear contribution acts as re-energization of the seed population produced by turbulent acceleration, shaping an effective powerlaw tail close to  $\propto \epsilon^{-3}$  (per number), therefore close to that inferred from IceCube observations. The parameters adopted here are the same as those adopted in Sec. 2.3 for what concerns the shear layer, and  $v_A = 0.20 c$ ,  $v_{\text{adv}} = 0.02 c$ ,  $\ell_c = 10 r_g$ ,  $r_{\text{co}} = 30 r_g$  as in Fig. 1 for stochastic acceleration. For simplicity, we ignored possible boosting effects for the shear contribution. In general, if the shear flow were sub-relativistic, shear acceleration would become too slow to have any effect, as quantified by the dependence of the diffusion coefficient on the Lorentz factor of the flow (Sec. 2.3). We also note that we have considered a scenario in which particles are injected at one boundary of the corona, accelerated by turbulence, and then advected into the shear layer. Had we considered that a fraction of particles could be advected into the black hole instead

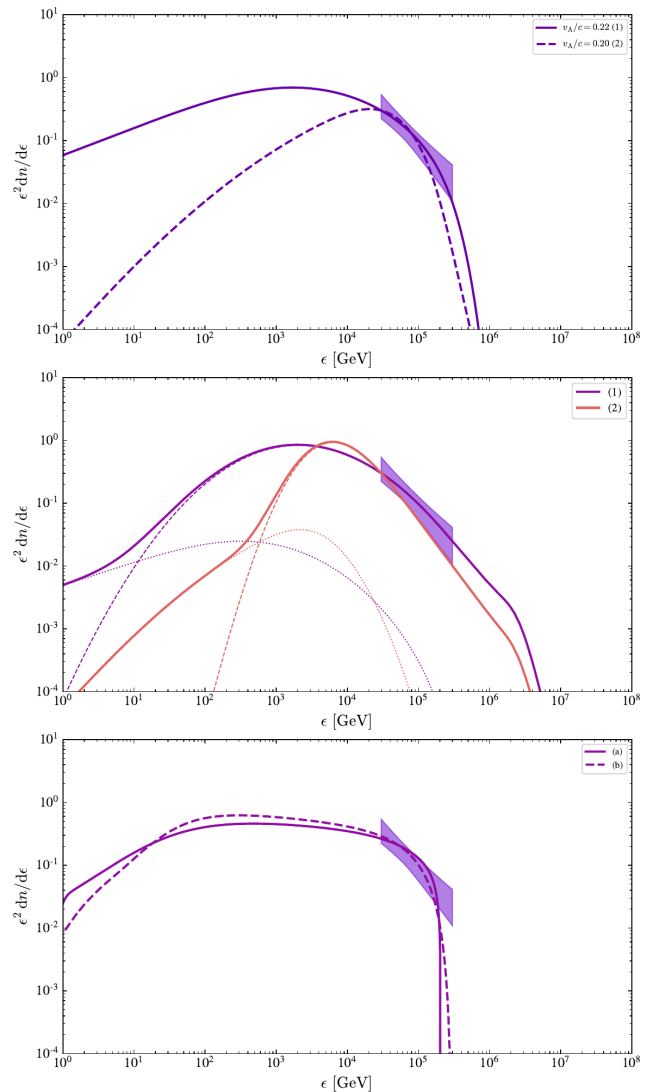


**Fig. 3.** Proton energy spectra  $du_p/d\ln \epsilon \equiv \epsilon^2 dn/d\epsilon$  vs proton energy  $\epsilon$  for three characteristic scenarios described in the text. For each panel, the energy density distribution is shown in units of the background plasma pressure. Top panel: stochastic acceleration in the turbulent corona, with characteristic Alfvénic velocity  $v_A \simeq 0.2 c$  (see text for details), for model (1) and (2), corresponding to solid and dashed lines respectively. Middle panel: combination of stochastic acceleration in the corona, with shear acceleration at the base of the jet, see text for the details of the physical parameters used. Here the stochastic contribution is indicated by dotted lines, the shear contribution by dashed lines and the sum of the two by solid lines. The different colors corresponds to model (1) and (2). For the top and middle panels, the normalization of the energy density in accelerated particles has been fixed in order to reproduce the inferred proton flux. Bottom panel: modelling of stochastic acceleration accounting for self-regulation by particle feedback on the turbulence (damping), for a characteristic Alfvénic velocity  $v_A \simeq 0.2 c$ . As discussed in the text, self-regulation occurs once the energy density becomes of order unity in the units of background plasma pressure. In this scenario, the flux has not been normalized by an ad hoc factor, the spectral shape is directly fixed by the influence of backreaction. The plasma  $\beta_p$  parameter is 0.5 (cf. Appendix A).

of the jet, the shear contribution would have been reduced. Similarly, had we assumed that particles were injected into stochastic acceleration uniformly throughout the corona (see Sec. 2.2, then the spectrum injected into the shear process would have been the steady-state spectrum  $dn_{\text{cor}}/d\epsilon$  instead of that discussed above.

In that case as well, the overall shear contribution would have been effectively reduced and, normalizing the overall spectrum to the inferred values without invoking boosting, would have implied stronger energy requirements. In the present case, the ratios of integrated energy density in suprathermal particles to background plasma pressure are, respectively, 4.1 and 2.7 for model (1) and (2).

Finally, we investigate the consequences of self-regulation of the acceleration process by turbulent damping. Given that in both scenarios discussed previously, the pressure carried by the accelerated particles is comparable to that in the background plasma, this last scenario appears quite likely. We also note that in the above cases, the flux normalization was set in such a way as to reproduce that inferred from IceCube observations, and that, as mentioned previously, this amounts to selecting a precise fraction of particles that are extracted out of the thermal pool and then accelerated to high energies. Here, we thus account for the back-reaction of the accelerated particles on the turbulence following the prescriptions of Lemoine et al. (2024). As detailed therein, backreaction becomes effective once the rate at which particles draw energy from the turbulent cascade exceeds that at which the cascade is replenished by energy injection. The former rate can be written  $\sim v_{\text{acc}} u_p$  ( $u_p$  the suprathermal proton energy density), with  $v_{\text{acc}} \sim v_A^2 / (c \ell_c)$ , while the latter reads  $\sim (v_A / \ell_c) u_B$  (with  $u_B$  the magnetic energy density), hence turbulent damping becomes effective once  $u_p / u_B \sim c / v_A$ . Assuming a plasma  $\beta_p$  unity (see App. A), this also means that damping takes place once  $u_p / p_{\text{gas}} \sim c / v_A \sim O(1)$  here. Once particles start to damp the turbulence, the stochastic acceleration rate stalls, and acceleration becomes self-regulated.

To fix parameters, we assume that the cascade rate on the outer scale is  $0.5 v_A / \ell_c$ , as expected on general grounds. We use as before  $r_{\text{co}} = 30 r_g$ ,  $v_{\text{adv}} = 0.02 c$  and  $\ell_c = 10 r_g$  and inject particles at  $\gamma_0 \sim 1$  as before, with an energy density a factor four below that contained in the magnetized turbulence. We then track their acceleration using two effective models (a) and (b) described in Lemoine et al. (2024), mimicking models (1) and (2) above. In detail, model (a) corresponds to the Fokker-Planck model and assumes  $v_A = 0.21 c$ , while model (b) describes advection in momentum space of a broken powerlaw spectrum assuming  $v_A = 0.28 c$ . Finally, we compute the global stationary spectrum over the corona by integrating the time-dependent spectra as in Eq. (3). The resulting spectrum is shown in the lower panel of Fig. 3. We stress that in the present scenario, no ad hoc normalization of the energy content has been adopted. This energy content is dictated by the backreaction of particles on the turbulence, which as discussed above, implies that the total energy density in suprathermal particles must be of the order of  $p_{\text{gas}} c / v_A$ . Indeed, in units of  $p_{\text{gas}}$ , the energy density associated to the particle spectra shown in Fig. 3 is 3.4 in model (a) and 4.1 in model (b). The general shape of the spectrum does not depend much on the method used to carry the integration. The key parameter that determines whether the overall flux can match the detailed spectrum at energies 30 – 300 TeV is the Alfvén velocity (more generally  $v_{\text{acc}} \tau_{\text{adv}}$ ), which determines the location of the high-energy cut-off. The fact that the inferred spectrum can be reproduced at the price of reasonable parameters, without an arbitrary normalization, provides additional support and motivation for this scenario.

The global spectral shape of self-regulated acceleration can be understood as follows. In a first stage, particles are accelerated as in the test-particle picture of the first scenario investigated previously in this section. This occurs as long as the energy carried by the suprathermal particles remains below the threshold for

backreaction and it explains the similarity of the spectral slopes at low energies with that seen in the upper panel of Fig. 3. Once feedback becomes efficient, acceleration stalls at the momentum determining the peak of the energy distribution, while particles of larger momenta can keep being accelerated because they interact with wavelength modes of larger scales, which have not yet been damped. This tends to shape time-dependent energy spectra that are approximately flat at high energies. The average of these time-dependent spectra over the crossing time of the corona, accounting for energy and escape losses, then shapes the spectrum observed, close or slightly steeper than  $-2$  in slope (per number). One phenomenological implication of this modelling is that, in order to match a spectrum steeper than  $-2$  in slope, the spectrum should be close to the cut-off region, i.e. revealing increasing curvature towards higher energies. For larger acceleration rates, or larger  $v_{\text{acc}} \tau_{\text{adv}}$ , the maximum energy is pushed to larger values, hence the spectrum in a given region comes closer to  $-2$  in slope.

One must therefore keep in mind the dependency of the location of the cut-off on  $v_{\text{acc}} \tau_{\text{adv}}$ . Although, were this combination of parameters inhomogeneous throughout the corona, e.g., because the Alfvénic velocity itself would vary in space (as proposed in the context of X-ray binaries, see Nättilä 2024), the sharp high-energy cut-off would be replaced by a softer dependence associated with the tail of values of  $v_{\text{acc}} \tau_{\text{adv}}$ . One is thus led to contemplate a more general interpretation of the proton spectrum, in which the flux level would be determined by backreaction as modelled above, while the slope of the spectrum in the region probed by IceCube would be dictated by the distribution of acceleration rates (and advection times) experienced by the particle population. We however defer the detailed investigation of such a scenario to future work.

## 4. Conclusions

In this paper, we have investigated scenarios of stochastic particle acceleration in a turbulent magnetized black hole corona and in the sheared velocity flow at the base of the jet to examine to what degree they can account for proton energies inferred from IceCube neutrino observations of the Seyfert prototype NGC 1068, namely  $\epsilon \sim 30 - 300$  TeV, as well as for the overall level of energy density. To do so, we have borrowed recent results regarding stochastic particle acceleration in turbulence and paid particular attention to the transport equation, i.e., we have considered the influence of turbulent transport on escape losses and incorporated advection losses as a time limit on particle acceleration (Sec. 2.2). In Sec. 3, we have confronted three characteristic scenarios to the proton spectrum inferred in the case of NGC 1068 to conclude the following.

In a first scenario, which portrays particle acceleration in the test-particle limit in a turbulent corona, we confirm previous results suggesting that a characteristic Alfvénic velocity  $v_A \simeq 0.1 - 0.2 c$  for a coherence length  $\ell_c \sim 3 - 10 r_g$  can reproduce the general shape of the spectrum observed. However, this comes at the cost of ad hoc normalization of the proton spectrum, up to an appreciable fraction of the background plasma pressure, in some cases exceeding unity. In terms of phenomenology, the spectrum is expected to reveal increasing curvature towards higher energies.

In a second scenario, we have investigated the possibility that stochastic acceleration would consume less energy, but be completed by a phase of re-acceleration in the sheared velocity flow at the base of a mildly relativistic jet. While such a scenario admittedly introduces new parameters into the problem, it shows



that shear re-acceleration can play a role and lead to a satisfactory fit to the observed spectrum for a reasonable choice of parameters. In particular, depending on the conditions for escape, the particle distribution could extend to even higher energies as shown in Fig. 3. In the present context, the relative importance of shear acceleration depends on the magnitude of the shear, which determines the rate at which particles are re-energized in the jet boundary layer, just as it depends on the advection velocity in the corona. Similarly to the first scenario, the overall flux normalization is freely chosen, and requires that the energy density in high-energy protons lies close to the overall background plasma pressure.

This apparent coincidence is intriguing with respect to particle injection into the stochastic process, because it means that one must extract a specific fraction of particles out of the thermal pool, orders of magnitude smaller than unity, yet such that after acceleration they carry an amount of energy comparable to the pressure of their parent population. Observing that the gas pressure is  $\beta_p$  (plasma beta parameter) times the magnetic energy density  $u_B$ , and that  $\beta_p \sim 1$ , this observation may indicate that the acceleration process is as efficient as can be, i.e., that the high-energy particles extract as much energy as they can from the turbulent cascade.

We have thus examined a third scenario, in which turbulent acceleration is self-regulated by this feedback, which takes the form of damping of the turbulent cascade on intermediate length scales (meaning, between the outer scale and the kinetic scales that lead to plasma heating). In this scenario, the problem is fixed by the rate at which turbulent energy is injected on the outer scale  $\ell_c$ , with generic value  $\sim u_B v_A / \ell_c$ . Adopting this rate and characteristic Alfvénic velocities as above, solving for the concomitant dynamical evolution of the turbulence and of the accelerated particles, we are able to reproduce the inferred proton spectra without having to specify the flux normalization. We have not explored the possibility that the accelerated particles could provide a backreaction at a more global – hydrodynamical – level on the structure of the flow itself, such as the lift off of the hydrostatic equilibrium in the corona or jet deceleration in the case of shear acceleration. Such issues obviously deserve further investigation.

This self-regulated acceleration process provides a natural means of achieving rough equipartition between the accelerated particles and the turbulent magnetic energy density. It becomes operative provided the fraction  $\chi_0$  of particles that are extracted out of the thermal pool and injected into stochastic acceleration verifies  $\chi_0 \gtrsim (v_A/c)^{-1} \beta_p^{-1} (\epsilon_{\max}/\bar{\epsilon}_{\text{th}})^{-1}$ , in terms of the plasma beta parameter  $\beta_p$ , the Alfvénic velocity  $v_A$  (here playing the role of the characteristic eddy velocity on the outer scale of the turbulence),  $\epsilon_{\max}$  the maximum energy of the non-thermal energy spectrum and  $\bar{\epsilon}_{\text{th}} \sim k_B T$  the mean thermal energy. If the injection fraction  $\chi_0$  is smaller than the above, feedback has not set in by the time particles are accelerated to  $\epsilon_{\max}$ , and hence particle acceleration proceeds as in a test-particle picture. However, if  $\epsilon_{\max}/\bar{\epsilon}_{\text{th}} \gg 1$ , i.e., if particles are able to reach high energies, feedback becomes natural and the high-energy part of the accelerated spectrum then depends weakly on the details of injection. In direct consequence of the above, the overall neutrino luminosity of the source is not only controlled by the X-ray luminosity that governs  $p - \gamma$  interactions, but also by the magnetic energy content.

Our study further indicates that other parameters are likely to influence the neutrino spectrum. We have notably remarked that the maximum energy is strongly sensitive to the acceleration rate, e.g., the Alfvén velocity, the coherence length, as well as

to the advection timescale through the corona. This dependence arises because the mean particle energy increases exponentially fast in turbulent acceleration, up to a number of e-folds that is set by a combination of these parameters. An important corollary of this is that different sources might exhibit different spectra. An alternative way of viewing this strong dependence is that, should the corona be inhomogeneous in terms of  $v_A$  (for instance), the final spectrum will be a sum of spectra obtained for differing  $v_A$ , or said otherwise, the final spectrum will be shaped by the distribution of  $v_A$  (and other parameters) in the corona. Overall, therefore, it is tempting to interpret the flux level as the consequence of self-regulated particle acceleration by turbulence damping (or possibly, viscous damping of the sheared velocity flow), and the general slope of the spectrum as given by the distribution of acceleration rates within the corona.

Finally, as pointed out to us by A. Beloborodov and A. Levinson, the backreaction of particles on the corona turbulence introduces new issues, as it may jeopardize the stochastic acceleration of electrons, which is expected to power the X-ray luminosity of the corona. We note however that, in the present description, the advection of particles through the corona effectively leads to stratification in terms of mean energy, as time-dependent spectra are also position-dependent. Therefore, close to the boundary where particles are injected into the corona, turbulence is left unscathed and electron acceleration is efficient. It suffices to accelerate them to Lorentz factors  $\gamma_e \lesssim 10^3$  to power the X-ray luminosity by Comptonization, and such electrons behave as mildly- or sub-relativistic protons. Therefore, it appears reasonable to assume that such electrons can indeed be accelerated to the energies required before turbulent damping becomes effective. A detailed investigation of this question will form the basis of future work.

*Acknowledgements.* It is a pleasure to thank A. Beloborodov and A. Levinson, F. Oikonomou and E. Peretti as well as the members of the CN-6 connector of the Munich Excellence Cluster ORIGINS (in particular, P. Padovani, X. Rodrigues, and E. Resconi) for stimulating discussions. FMR acknowledges support by a DFG grant (RI 1187/8-1) and the kind hospitality of the IAP Paris.

## Appendix A: Modelling the loss and escape rates

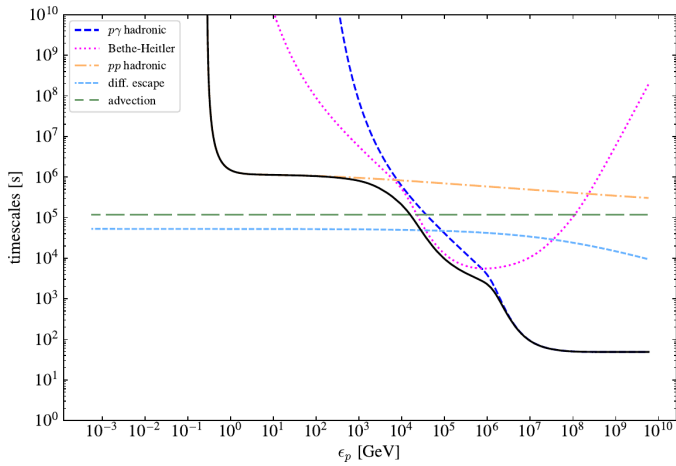


**Fig. A.1.** Energy losses for:  $L_{\text{disk}} = 5 \times 10^{44}$  erg/s,  $L_X = 0.8 \times 10^{44}$  erg/s,  $\Gamma_X = 1.95$ ,  $\epsilon_{X,\text{max}} = 128$  keV,  $r_{\text{co}} = 30 r_g$ ,  $r_g = 2.35 \times 10^{12} M_{7.2}$  cm,  $B = 10^3$  G,  $n_p = 10^9$  cm $^{-3}$ . The diffusive escape time is shown for  $v_A = 0.2 c$ , while the advection time assumes  $v_{\text{adv}} = 0.02 c$  (as expected for the radial inflow velocity at  $r_{\text{co}}$  with viscosity parameter  $\alpha = 0.1$ ).

We implement energy and escape losses as follows. While the advection timescale  $\tau_{\text{adv}}$  is momentum-independent,  $\tau_{\text{esc}} \approx r_{\text{co}}^2/2\kappa$  depends on momentum through the spatial diffusion coefficient  $\kappa$ . We model transport as a combination of turbulent advection with effective diffusion coefficient  $\kappa_{\text{turb}} = \ell_c v_A/3$ , and scattering on magnetic inhomogeneities with mean free path  $\lambda_{\text{scatt}} = r_L^{1/3} \ell_c^{2/3}$ , see e.g. [Berezinskii et al. \(1990\)](#), or [Lemoine \(2023\)](#) and [Kempski et al. \(2023\)](#) for recent discussions. Correspondingly, we set  $\kappa \equiv \kappa_{\text{turb}} + \lambda_{\text{scatt}} c/3$ . As discussed in the main text, this implies that particle escape is mostly governed by turbulent transport in the energy interval of phenomenological relevance, see Fig. A.1 for an illustration with our fiducial parameters  $\ell_c = 10 r_g$ ,  $v_A = 0.2 c$ ,  $r_{\text{co}} = 30 r_g$  and  $B = 10^3$  G. Note that, when computing shear acceleration, we neglect the effect of turbulent transport, which corresponds to the assumption that the turbulence in the sheared region is not strongly dynamic.

To model radiative losses, we consider a disk emission represented by a multi-color black-body  $L_\epsilon \propto \epsilon^{4/3} \exp(-\epsilon/\epsilon_{\text{cd}})$  for  $\epsilon > 0.1 \epsilon_{\text{cd}}$  and  $L_\epsilon \propto \epsilon^3$  for  $\epsilon < 0.1 \epsilon_{\text{cd}}$ . The disc cut-off is  $\epsilon_{\text{cd}} = 31.5$  eV. The integrated disk luminosity is  $L_{\text{disk}} = 5 \times 10^{44}$  erg/s. The X-ray emission is a powerlaw  $L_\epsilon \propto \epsilon^{-1-x} \exp(-\epsilon/\epsilon_{\text{cX}})$  for  $\epsilon > \epsilon_{\text{cX}}$  (i.e. above the disk cut-off energy), and  $L_\epsilon \propto \epsilon^2$  below. The X-ray cut-off is set at  $\epsilon_{\text{cX}} = 128$  keV and the integrated luminosity  $L_X = 0.8 \times 10^{44}$  erg/s.

We assume a black hole of mass  $M_{\text{BH}} = 10^{7.2} M_\odot$ , and corresponding gravitational radius  $r_g \approx 2.35 \times 10^{12} M_{7.2}$  cm (Schwarzschild radius  $r_s = 2r_g$ ). The Eddington reference luminosity is  $L_{\text{Edd}} = 2 \times 10^{45} M_{7.2}$  erg/s. We note that for NGC 1068, the all-flavour, integrated (1.5-15 TeV) isotropic-equivalent neutrino luminosity is of order  $L_\nu \approx 10^{42} (d/10 \text{ Mpc})^2$  erg/s  $\sim L_{\text{Edd}}/10^3$ , and the estimated bolometric luminosity  $L_{\text{bol}} \sim 5 \times 10^{44}$  erg/s (e.g., [IceCube Collaboration et al. 2022](#); [Padovani et al. 2024](#)). We take  $r_{\text{co}} = 30 r_g$  for the equatorial extension of the corona. The thermal background proton number density is set to  $n_{\text{th}} = 2 \times 10^9$  cm $^{-3}$ , corresponding to a plasma beta  $\beta_p \sim 1$  (we use 1 everywhere). Advective escape (radial inflow) in the corona is parameterized by  $v_{\text{adv}}$ , where we take  $v_{\text{adv}} = \alpha_d v_k(r_{\text{co}})$  as reference value, with  $v_k(r)$  the Keplerian velocity and  $\alpha_d \approx 0.1$  the viscosity parameter.

Figure A.1 presents the energy losses timescales corresponding to the above background photon spectral energy distribution. For comparison, for the chosen parameters, the required cosmic-ray power for a NGC 1068 type source is of order  $L_{\text{CR}} \sim L_\nu (ct_{\text{cool}}/r_{\text{co}}) \sim (5 - 10) \times 10^{43}$  erg/s, equivalent to an energy density of  $u_{\text{CR}} \approx L_{\text{CR}}/(4\pi r_{\text{co}}^2 c) \sim (3 - 6) \times 10^4$  erg/cm $^3$  and comparable to the energy density  $u_B \approx 4 \times 10^4$  erg/cm $^3$  of the magnetic field.

## References

- Abbasi, R., Ackermann, M., Adams, J., et al. 2024a, arXiv e-prints, arXiv:2406.06684
- Abbasi, R., Ackermann, M., Adams, J., et al. 2024b, arXiv e-prints, arXiv:2406.07601
- Aharonian, F. & Neronov, A. 2005, *ApJ*, 619, 306
- Aharonian, F. A., Belyanin, A. A., Derishev, E. V., Kocharovskiy, V. V., & Kocharovskiy, V. V. 2002, *Phys. Rev. D*, 66, 023005
- Ambrosone, A. 2024, arXiv e-prints, arXiv:2406.13336
- Beloborodov, A. M. 1999, *MNRAS*, 305, 181
- Berezinskii, V. S., Bulanov, S. V., Dogiel, V. A., & Ptuskin, V. S. 1990, *Astrophysics of cosmic rays* (Amsterdam: North-Holland, 1990, edited by Ginzburg, V.L.)
- Berezinskii, V. S. & Ginzburg, V. L. 1981, in *International Cosmic Ray Conference*, Vol. 1, International Cosmic Ray Conference, 238
- Bresci, V., Lemoine, M., Gremillet, L., et al. 2022, *Phys. Rev. D*, 106, 023028
- Brunetti, G. & Lazarian, A. 2016, *Mon. Not. R. Astron. Soc.*, 458, 2584
- Comisso, L. & Sironi, L. 2018, *Phys. Rev. Lett.*, 121, 255101
- Comisso, L. & Sironi, L. 2019, *Astrophys. J.*, 886, 122
- Comisso, L. & Sironi, L. 2022, *ApJ*, 936, L27
- Das, A., Zhang, B. T., & Murase, K. 2024, *ApJ*, 972, 44
- De Villiers, J.-P., Hawley, J. F., & Krolik, J. H. 2003, *ApJ*, 599, 1238
- De Villiers, J.-P., Hawley, J. F., Krolik, J. H., & Hirose, S. 2005, *ApJ*, 620, 878
- Demidem, C., Lemoine, M., & Casse, F. 2020, *Phys. Rev. D*, 102, 023003
- Dermer, C. D., Miller, J. A., & Li, H. 1996, *ApJ*, 456, 106
- Dexter, J. & Begelman, M. C. 2024, *MNRAS*, 528, L157
- Di Matteo, T., Blackman, E. G., & Fabian, A. C. 1997, *MNRAS*, 291, L23
- Eichler, D. 1979a, *ApJ*, 232, 106
- Eichler, D. 1979b, *Astrophys. J.*, 229, 413
- Eichmann, B., Oikonomou, F., Salvatore, S., Dettmar, R.-J., & Tjus, J. B. 2022, *ApJ*, 939, 43
- Eilek, J. A. 1979, *Astrophys. J.*, 230, 373
- Fabian, A. C., Lohfink, A., Kara, E., et al. 2015, *MNRAS*, 451, 4375
- Fang, K., Lopez Rodriguez, E., Halzen, F., & Gallagher, J. S. 2023, *ApJ*, 956, 8
- Farrar, G. R. & Piran, T. 2014, arXiv e-prints, arXiv:1411.0704
- Fiorillo, D. F. G., Comisso, L., Peretti, E., Petropoulou, M., & Sironi, L. 2024a, arXiv e-prints, arXiv:2407.01678
- Fiorillo, D. F. G., Petropoulou, M., Comisso, L., Peretti, E., & Sironi, L. 2024b, *ApJ*, 961, L14
- Gallimore, J. F., Baum, S. A., O’Dea, C. P., & Pedlar, A. 1996, *ApJ*, 458, 136
- Guépin, C., Kotera, K., Barausse, E., Fang, K., & Murase, K. 2018, *A&A*, 616, A179
- Halzen, F. 2023, arXiv e-prints, arXiv:2305.07086
- IceCube Collaboration, Abbasi, R., Ackermann, M., et al. 2022, *Science*, 378, 538
- Inoue, Y. & Doi, A. 2018, *ApJ*, 869, 114
- Inoue, Y., Khangulyan, D., & Doi, A. 2020, *ApJ*, 891, L33
- Inoue, Y., Takasao, S., & Khangulyan, D. 2024, *PASJ*, 76, 996
- Islaker, H., Vlahos, L., & Constantinescu, D. 2017, *Phys. Rev. Lett.*, 119, 045101
- Kakuwa, J. 2016, *Astrophys. J.*, 816, 24
- Kammoun, E., Lohfink, A. M., Masterson, M., et al. 2024, *Frontiers in Astronomy and Space Sciences*, 10, 1308056
- Kamraj, N., Brightman, M., Harrison, F. A., et al. 2022, *ApJ*, 927, 42
- Kamraj, N., Harrison, F. A., Baloković, M., Lohfink, A., & Brightman, M. 2018, *ApJ*, 866, 124
- Kara, E., García, J. A., Lohfink, A., et al. 2017, *MNRAS*, 468, 3489
- Kardashev, N. S. 1962, *Soviet Ast.*, 6, 317
- Kempski, P., Fielding, D. B., Quataert, E., et al. 2023, *MNRAS*, 525, 4985
- Kheirandish, A., Murase, K., & Kimura, S. S. 2021, *ApJ*, 922, 45
- Kimura, S. S., Murase, K., & Mészáros, P. 2019a, *Phys. Rev. D*, 100, 083014
- Kimura, S. S., Tomida, K., & Murase, K. 2019b, *MNRAS*, 485, 163
- King, A. L., Lohfink, A., & Kara, E. 2017, *ApJ*, 835, 226
- Lemoine, M. 2019, *Phys. Rev. D*, 99, 083006
- Lemoine, M. 2021, *Phys. Rev. D*, 104, 063020
- Lemoine, M. 2022, *Phys. Rev. Lett.*, 129, 215101
- Lemoine, M. 2023, *Journal of Plasma Physics*, 89, 175890501
- Lemoine, M. & Malkov, M. A. 2020, *Mon. Not. R. Astron. Soc.*, 499, 4972

- Lemoine, M., Murase, K., & Rieger, F. 2024, *Phys. Rev. D*, 109, 063006
- Lenain, J. P., Ricci, C., Türler, M., Dorner, D., & Walter, R. 2010, *A&A*, 524, A72
- Levinson, A. & Boldt, E. 2002, *Astroparticle Physics*, 16, 265
- Liska, M. T. P., Musoke, G., Tchekhovskoy, A., Porth, O., & Beloborodov, A. M. 2022, *ApJ*, 935, L1
- Litvinenko, Y. E. 2012, *Astron. Astrophys.*, 544, A94
- Liu, B. F., Mineshige, S., & Shibata, K. 2002, *ApJ*, 572, L173
- Lynn, J. W., Quataert, E., Chandran, B. D. G., & Parrish, I. J. 2014, *Astrophys. J.*, 791, 71
- Malzac, J., Beloborodov, A. M., & Poutanen, J. 2001, *MNRAS*, 326, 417
- Mbarek, R., Philippov, A., Chernoglazov, A., Levinson, A., & Mushotzky, R. 2024, *Phys. Rev. D*, 109, L101306
- Merloni, A. & Fabian, A. C. 2001, *MNRAS*, 321, 549
- Merloni, A. & Fabian, A. C. 2002, *MNRAS*, 332, 165
- Murase, K. 2022, *ApJ*, 941, L17
- Murase, K., Karwin, C. M., Kimura, S. S., Ajello, M., & Buson, S. 2024, *ApJ*, 961, L34
- Murase, K., Kimura, S. S., & Mészáros, P. 2020a, *Phys. Rev. Lett.*, 125, 011101
- Murase, K., Kimura, S. S., Zhang, B. T., Oikonomou, F., & Petropoulou, M. 2020b, *ApJ*, 902, 108
- Nättilä, J. 2024, *Nature Communications*, 15, 7026
- Neronov, A., Savchenko, D., & Semikoz, D. V. 2024, *Phys. Rev. Lett.*, 132, 101002
- Padovani, P., Resconi, E., Ajello, M., et al. 2024, *Nature Astronomy*, 8, 1077
- Pecora, F., Servidio, S., Greco, A., et al. 2018, *J. Plasma Phys.*, 84, 725840601
- Pezzi, O., Blasi, P., & Matthaeus, W. H. 2022, *ApJ*, 928, 25
- Poutanen, J., Veledina, A., & Beloborodov, A. M. 2023, *ApJ*, 949, L10
- Protheroe, R. J. & Szabo, A. P. 1992, *Phys. Rev. Lett.*, 69, 2885
- Pugliese, F., Brodiano, M., Andrés, N., & Dmitruk, P. 2023, *ApJ*, 959, 28
- Rieger, F. M. 2019, *Galaxies*, 7, 78
- Rieger, F. M. & Aharonian, F. A. 2009, *A&A*, 506, L41
- Rieger, F. M. & Duffy, P. 2019, *ApJ*, 886, L26
- Rieger, F. M. & Duffy, P. 2022, *ApJ*, 933, 149
- Rieger, F. M. & Mannheim, K. 2000, *A&A*, 353, 473
- Rieger, F. M. & Mannheim, K. 2002, *A&A*, 396, 833
- Roy, A. L., Wilson, A. S., Ulvestad, J. S., & Colbert, J. M. 2000, in *EVN Symposium 2000, Proceedings of the 5th European VLBI Network Symposium*, ed. J. E. Conway, A. G. Polatidis, R. S. Booth, & Y. M. Pihlström, 7
- Salvatore, S., Eichmann, B., Rodrigues, X., Dettmar, R. J., & Becker Tjus, J. 2024, *A&A*, 687, A139
- Schlickeiser, R. 1984, *Astron. Astrophys.*, 136, 227
- Schlickeiser, R. 1989, *ApJ*, 336, 243
- Sioulas, N., Isliker, H., & Vlahos, L. 2020a, *Astrophys. J.*, 895, L14
- Sioulas, N., Isliker, H., Vlahos, L., Koumtzis, A., & Pisokas, T. 2020b, *Mon. Not. R. Astron. Soc.*, 491, 3860
- Sironi, L. & Beloborodov, A. M. 2020, *ApJ*, 899, 52
- Stern, B. E., Poutanen, J., Svensson, R., Sikora, M., & Begelman, M. C. 1995, *ApJ*, 449, L13
- Trotta, D., Franci, L., Burgess, D., & Hellinger, P. 2020, *ApJ*, 894, 136
- Wang, J., Rieger, F. M., & Mizuno, Y. 2024, *ApJ*, 967, 36
- Wang, J.-S., Reville, B., Mizuno, Y., Rieger, F. M., & Aharonian, F. A. 2023, *MNRAS*, 519, 1872
- Waxman, E. 2024, Talk given at RICAP 24
- Webb, G. M., Xu, Y., Biermann, P. L., et al. 2023, *ApJ*, 958, 169
- Werner, G. R., Uzdensky, D. A., Begelman, M. C., Cerutti, B., & Nalewajko, K. 2018, *MNRAS*, 473, 4840
- Winter, W. & Lunardini, C. 2023, *ApJ*, 948, 42
- Wong, K., Zhdankin, V., Uzdensky, D. A., Werner, G. R., & Begelman, M. C. 2020, *Astrophys. J.*, 893, L7
- Xu, S. & Lazarian, A. 2023, *ApJ*, 942, 21
- Zdziarski, A. A. 1985, *ApJ*, 289, 514
- Zhdankin, V., Uzdensky, D. A., Werner, G. R., & Begelman, M. C. 2019, *Phys. Rev. Lett.*, 122, 055101
- Zhdankin, V., Werner, G. R., Uzdensky, D. A., & Begelman, M. C. 2017, *Phys. Rev. Lett.*, 118, 055103